Case Studies in Nondestructive Testing and Evaluation 2 (2014) 77–83

Contents lists available at ScienceDirect

Case Studies in Nondestructive Testing and Evaluation

www.elsevier.com/locate/csndt

# Deconvolution processing for improved acoustic wavefield imaging

Christian Kexel, Jochen Moll *

*Goethe University of Frankfurt, Department of Physics, Max-von-Laue-Strasse 1, 60438 Frankfurt am Main, Germany*

ARTICLE INFO

*Article history:*
Available online 29 October 2014

ABSTRACT

Sparse sensor networks for Lamb wave-based structural health monitoring (SHM) can detect defects in plate-like structures. However, the limited number of sensor positions provides little information to characterize the unknown scatterer. This can be achieved by full wavefield analysis e.g. using Laser Doppler vibrometry measurements.
This paper proposes deconvolution processing that enhances the acoustic wavefield interpretation by increasing the temporal resolution of the underlying ultrasound signals. Applying this preprocessor to the whole wavefield allows improved non-destructive assessment of the defect. This approach is verified experimentally through a case study on an isotropic aluminum plate with four cracks.


## 1. Introduction

Guided waves, such as Lamb waves, have demonstrated a high sensitivity towards defect detection in metallic and fiber-reinforced structures. They can be easily generated and sensed by means of permanently installed and low-cost piezoelectric wafer active sensors (PWAS). The geometry of the structure as well as the material properties and the bandwidth of the excitation signal decide whether only the fundamental or also higher wave modes propagate simultaneously. In permanent installations, the transducers are typically arranged in a sparse array configuration either in a distributed network [1,2] or concentrated phased-array type arrangement [3]. Both approaches have in common that a relatively low number of PWAS can be employed, which is advantageous in terms of system complexity, costs and weight considerations. A drawback of this sparse array technique is the restricted ability to characterize the defect since only insufficient information about wave scattering becomes available due to the limited number of measurement positions.

As soon as the location of the scatterer has been identified through a sparse array technique such as time-of-flight analysis [4] or digital beamforming [5], the scatterer can be characterized by measuring the full wavefield at a high number of scanning points in the direct neighbourhood of the scatterer. This can be achieved in a non-contact way by using either Laser-Doppler vibrometry [6], scanning air-coupled ultrasound [7] or scanning laser-induced ultrasound [8]. In practical applications, the existing PWAS can be exploited as wave sources. The full wavefield provides rich information about the scatterer that can be used either for acoustic wavefield imaging (AWI) [9–12], frequency–wavenumber analysis [13,14], local wave-number estimation techniques [8,15] or defect imaging via digital beamforming [16].

The motivation of this work is to enhance the performance of AWI by a compressed sensing (CS) deconvolution filter, where each ultrasound signal is represented by a spike train with high resolution in the time-domain, leading to improved

* Tel.: +49 (0) 69 798 47208.
*E-mail address:* moll@physik.uni-frankfurt.de (J. Moll).
*URL:* http://www.jochenmoll.de (J. Moll).

http://dx.doi.org/10.1016/j.csndt.2014.10.002
2214-6571/

and simplified diagnostics of the wavefield. Therefore, a CS-based deconvolution framework has been established, where the ultrasound signal is considered to be sparse in the domain of the excitation signal. Given by the model-based strategy, the technique can be applied not only to signals from metallic structures where the dispersion relation of the Lamb modes is well-known. By means of a suitable dictionary it is possible to apply the method to fiber-reinforced structures, too. In the framework of SHM, deconvolution of guided wave signals have been demonstrated in [17,18]. In the context of ultrasound non-destructive testing (NDT) several sparse deconvolution strategies have been proposed [19–21]. Recent developments in sparse signal processing in ultrasound NDT are reviewed in [22].

The remainder of the paper is organized as follows: Section 2 presents the theoretical background of the proposed CS deconvolution strategy and its numerical implementation. After that, Section 3 demonstrates its performance in a case study performed on an aluminum plate using full wavefield data obtained from a scanning Laser-Doppler-vibrometer (SLDV). The results from the CS-framework is compared against classical AWI-techniques, where the wavefield animation is based on the radio-frequency and envelope-detected waveforms, respectively. Finally, the main achievements will be summarized in the Conclusions.

## 2. Deconvolution of Lamb wave signals

The emerging field of compressed sensing (CS) is rather broad and has a multitude of applications [23,24]. Hence, it is important to specify in what variant compressed sensing is used. In this paper, we will consider CS in terms of a sparse signal reconstruction and deconvolution technique of time-varying Lamb wave signals.

### 2.1. Compressed sensing based deconvolution

Acoustic wave field imaging relies on a measured time-domain signal, denoted by $\vec{s}_{xy} = s(t)$, for every measurement position $(x, y)$ on the structure. In classical wavefield imaging, we arrive directly at snapshots of the wavefield, namely a two-dimensional map for every point in time $t \in \{1, \ldots, M\}$. In this paper, we introduce however an intermediate processing scheme that yields enhanced wavefield imaging.

We consider a measured signal $s(t) = \sum_{\tau=1}^{M-N} h(\tau) \cdot \chi(t-\tau)$ to be the convolution of a pulse waveform $\vec{h}$ and an unknown spike train $\vec{\chi}$ of length $N$. This means that the signal is a superposition of the original excitation pulse and its echoes that undergo attenuation and phase alteration during propagation through the structure. Due to attenuation and phase uncertainty $\vec{h}$ can in general assume the shape of several different waveforms with varying amplitude and phase relations. The convolution, involving several possible waveforms, can be specified as a linear system of equations $\vec{s} = \mathbf{A} \cdot \vec{\chi}$. Here, the so-called dictionary $\mathbf{A} = (a_{mn}) = (\vec{a}_1 \cdots \vec{a}_N)$ contains one distinct waveform at one distinct point in time in one of its columns $\vec{a}_n$. The columns are referred to as atoms.

In general, the $M \times N$ matrix $\mathbf{A}$ can have the property of $M < N$. Moreover, measurement noise and unconsidered effects might be present that require the addition of a noise term

$$\vec{s} = \mathbf{A} \cdot \vec{\chi} + \vec{\eta} \tag{1}$$

We thus find that the linear system of equations is underdetermined, yielding no unique solution. Hereafter, the task of recovering $\vec{\chi}$ is referred to as deconvolution. Sparse deconvolution based on compressed sensing mitigates these restrictions by imposing additional constraints. If we assume the measured time-domain signal to contain only a small number $K$ of relevant pulses, the solution $\vec{\chi}$ becomes sparse. We refer to $K$ as sparsity or sparsity level that satisfies $K \ll N$ in order to be considered sparse. This sparsity assumption is adequate for an experimental scenario where the original excitation pulse is scattered and reflected only few times.

The sparsity assumption finally yields an optimization problem that is widely studied in the field of compressed sensing:

$$\min_{\vec{\chi}} \|\vec{s} - \mathbf{A} \cdot \vec{\chi}\|_2 \quad \text{subject to } \|\vec{\chi}\|_0 \leq K \tag{2}$$

Here, $\|\cdot\|_2$ denotes the Euclidean norm and $\|\cdot\|_0$ denotes the $\ell_0$-pseudonorm that corresponds to the number of non-zero vector entries.

### 2.2. Numerical implementation

For a given signal, a suitable dictionary and a given sparsity level $K$, finding a solution of problem (2) requires in general a combinatorial computational effort. Hence, there are numerous faster algorithm in compressed sensing to approximate a solution to this problem. A main distinction can be drawn between relaxation and greedy approaches [25]. Relaxation schemes replace the $\ell_0$-norm with the $\ell_1$-norm in order to arrive at an easier convex optimization task that nevertheless delivers, under certain circumstances, suitable results. In this paper, we apply a greedy scheme. Orthogonal Matching Pursuit (OMP) [26,27] is such a method that seeks in a greedy manner at each step a locally optimal solution. At each step an atom is picked that correlates most with the measurement or subsequently with its residual. The OMP-algorithm is presented in detail in Ref. [26].

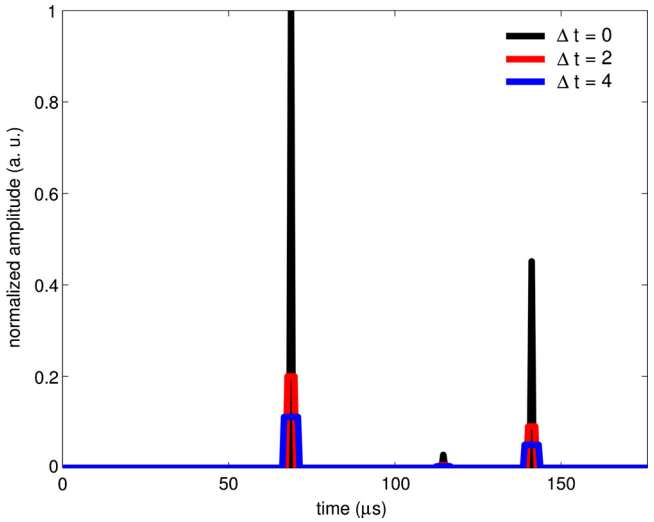


**Fig. 1.** Exemplary smoothed sparse solution (sparsity $K = 3$) for distinct parameters of the centered moving average filter. The lag $\Delta t = 0$ corresponds to the absence of any smoothing.

For a set of measurements and a given deconvolution algorithm, in our case OMP, the remaining task is to choose an appropriate dictionary matrix **A**. Since the properties of the excitation pulse, such as the excitation spectrum and the pulse duration (width), are known, we can model atoms of the dictionary to be similar pulses, but at different points of time. Since the phase behaviour for scattered and reflected waves is rather less known, we resort to looking at amplitude envelopes of signals. Hereafter, the amplitude envelope of a signal is denoted by $s_{\text{envelope}}(t) = \|s(t) + iH(s(t))\|_2$ where $H(s(t))$ is the Hilbert transform of signal $s(t)$. In our approach, the measured signal is replaced by its amplitude envelope and the dictionary contains the amplitude envelope of time-varying, modeled excitation pulses.

The final step in our numerical implementation is a smoothing filter: The solution of the deconvolution via OMP is the sparse spike train $\vec{\chi}$. It is a sparse representation of the measured signal $\vec{s}$. In order to get an enhanced wavefield image, we replace the original measurement by its sparse counterpart. The resulting sharp intensity peaks in the wavefield image of the monitored structure are sometimes hard to grasp visually. So we smooth the spike train using a standard moving average filter to obtain a comfortable, more coherent wavefield image while keeping most of the improved visualization of our approach. The centered moving average filter with discrete lag parameter $\Delta t$ yields a smoothed spike train

$$\chi_{\text{smooth}}(t) = \frac{\chi(t) + \sum_{\tau=1}^{\Delta t} \chi(t \pm \tau)}{2 \cdot \Delta t + 1} \tag{3}$$

where summation is also carried out over discrete time steps $\tau$. The impact of our filter on a sparse solution $\vec{\chi}$ is shown illustratively in Fig. 1 for different values of the lag $\Delta t$. A schematic representation (flowchart) of our whole implementation is depicted in Fig. 2.

## 3. Case study

In this paper, we consider a circular PWAS with a diameter of 10 mm as wave source that is placed in the middle of an aluminum plate that has the dimension 540 mm × 543 mm and a thickness of 1.5 mm. Four cracks each having a length of 30 mm have been introduced. A standard SLDV-setup, which has been proposed in [9], records a total number of 32,942 ultrasound signals at an equidistant grid of approximately 3 mm in horizontal and vertical plate direction. The excitation signal is a Hann-modulated tone-burst with five cycles at a carrier frequency of 120 kHz. This narrowband excitation signal minimizes the effect of dispersion. At this product of frequency and thickness the out-of-plane component of the fundamental symmetric Lamb mode is too small to be measured with the SLDV, so that the subsequent analysis is limited to the fundamental antisymmetric wave mode.

### 3.1. Deconvolution of Lamb-wave signals

To demonstrate the concept of the proposed technique, we first consider only a single measurement position on the plate for exemplary purposes. The measured time-domain signal is depicted on the top right-hand side of Fig. 2. It consists mainly of two waveforms of different amplitude and phase. Moreover, a low level of noise is present in the measurement. The dictionary is constructed of envelopes of modeled 120 kHz pulses with suitable widths. Exemplary atoms are depicted on the left-hand side of Fig. 2. Also pulses with slightly varying widths were tested and it was found that no close connection to the overall results exists.

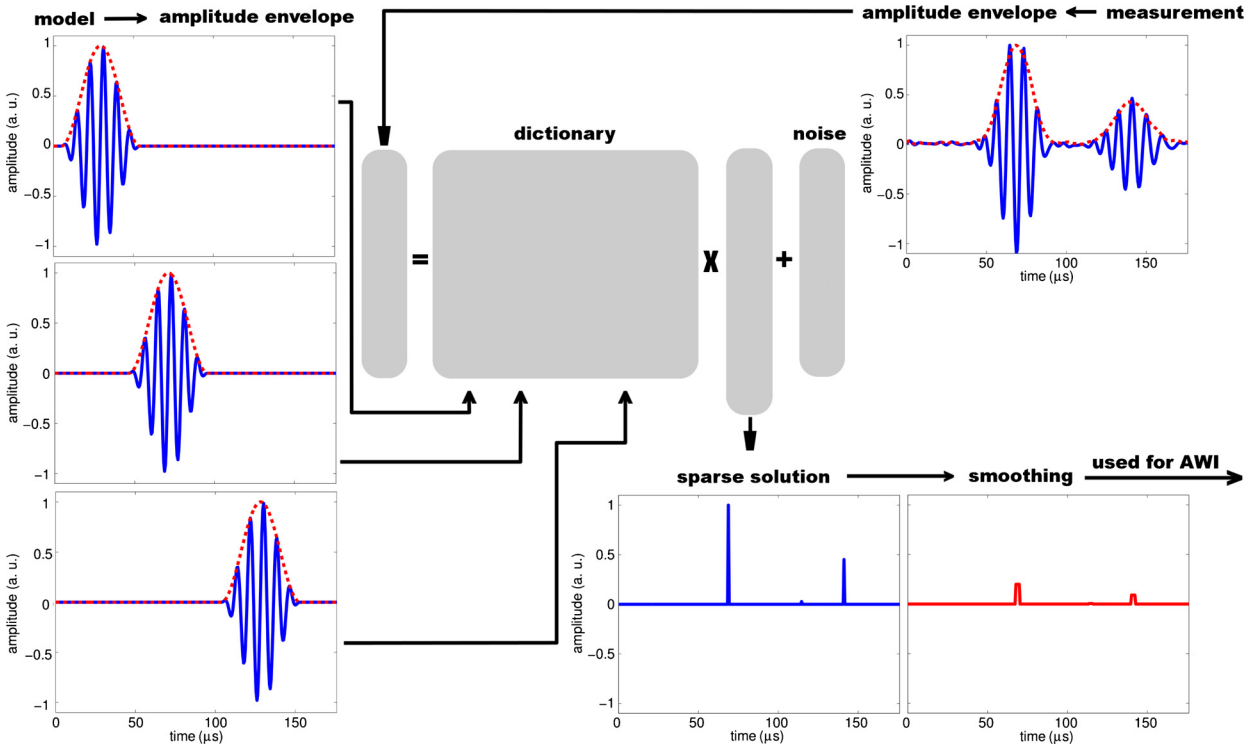


**Fig. 2.** Illustrative sketch of our deconvolution approach. The terms of Eq. (1) are depicted by exemplary signals.

Deconvolution was carried out with OMP and a sparsity level $K = 3$. The result is shown on the bottom of Fig. 2. The spike train consists of 3 non-zero entries. The smallest peak is almost completely smoothed out by the filter. We use a lag $\Delta t = 3$ in our studies within this work. By this choice, on the one side a considerable smoothing is achieved in order to yield a coherent resulting wavefield. On the other side the compact representation of the resulting wavefield is maintained, which can be destroyed otherwise for larger lags. This corresponds to a time window of 1.56 µs before and 1.56 µs after a certain point in time.

This example allows for two interesting observations: First, OMP accounts by default for the correct amplitudes during deconvolution. The relative amplitude of different pulses in the measurement is also preserved in the deconvolved result. Hence, there is no need to insert modeled pulses with different amplitudes into the dictionary matrix. The computational performance of OMP is closely linked to the size of the dictionary. It is of great importance to keep this matrix as small as possible.

Second, the sparsity $K$ is a user-defined parameter and by setting $K = 3$, we overestimated the number of pulses in the measurement. Since the exact number of echoes is usually not known in advance, such estimation problems occur quite frequently in compressed sensing frameworks. How to set unknown parameters in similar applications, is object of current research [28]. In our approach, the additional peak in the deconvolution result has a small value, because no obvious pulse in the measurement corresponds to it. Via the subsequent smoothing operation, the additional peak finally disappears. Mildly overestimating the sparsity of the scenario is not a critical issue in our approach. We also investigate and reconsider this issue in Section 3.3.

### *3.2. Conventional acoustic wavefield methods*

The whole wavefield is investigated using classical acoustic wavefield imaging (AWI) as shown in Fig. 3(a)–(b). The scatterer on the top left and the scatterer on the bottom right generate reflections that show their position as well as their orientation. The scatterer on the top right reflects the initial wave and thus the reflections interfers with the initial wave. Due to the interference of both waves, at least a localization of the scatterer is possible. The scatterer at the bottom of the left-hand side shows little interaction with the propagating Lamb-wave pulse.

### *3.3. Enhanced acoustic wavefield imaging via compressed sensing based deconvolution*

Next, the wavefield using the enhanced imaging scheme is studied. We employ the aforementioned method based on deconvolution and replace the measured signal with its smoothed sparse representation. Different choices of the user-defined parameter $K$ are tested, namely $K = 3$ as well as $K = 5$ and $K = 7$. The results are depicted in Fig. 3(c)–(e).

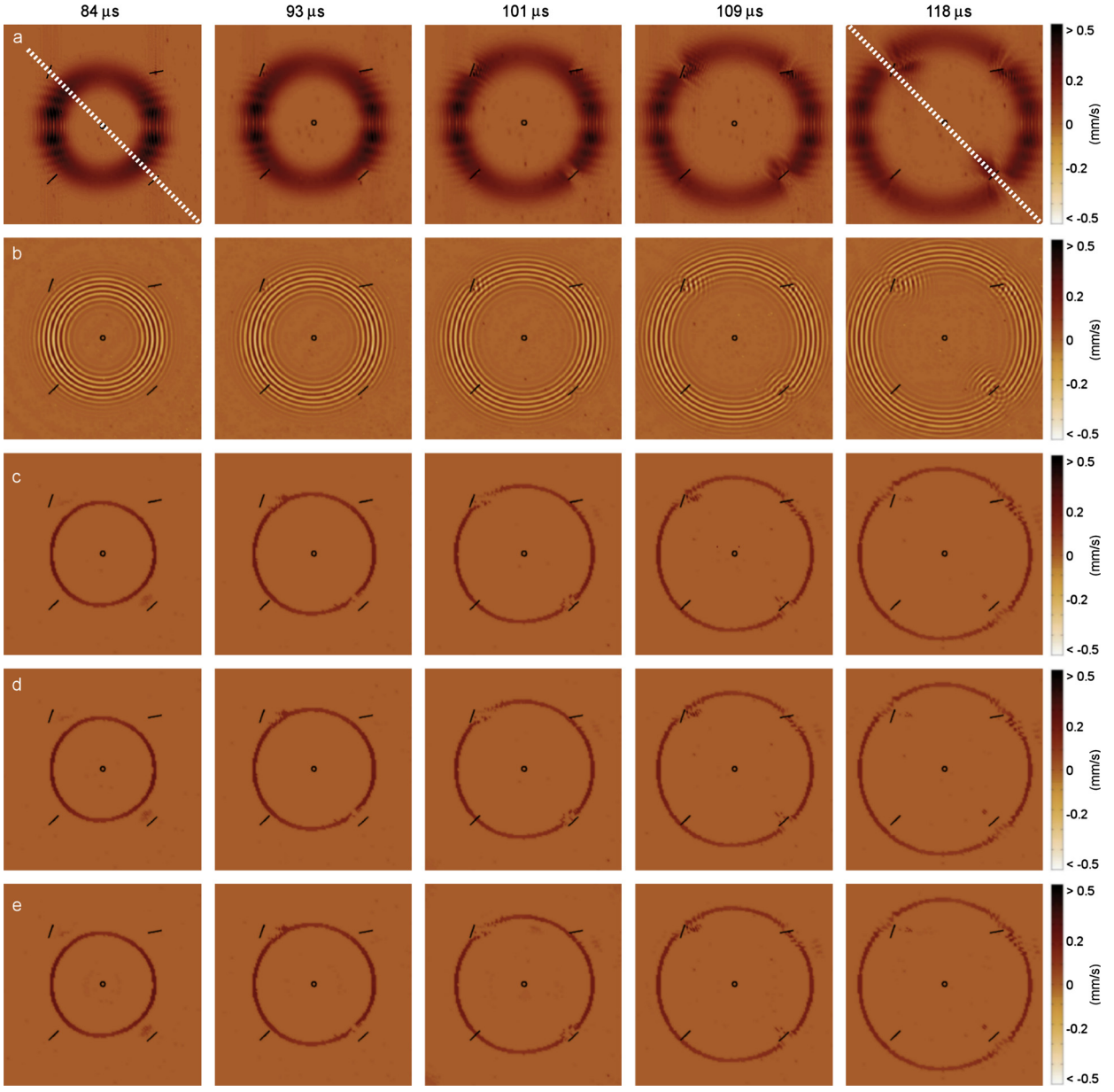


**Fig. 3.** Comparing the time-evolution of wavefields using different methods. *Row a:* Classical wavefield imaging using the amplitude envelope instead of original measured signal. *Row b:* Classical wavefield imaging using the raw radio-frequency signals. *Row c:* Enhanced wavefield imaging with sparsity $K = 3$. *Row d:* Enhanced wavefield imaging with sparsity $K = 5$. *Row e:* Enhanced wavefield imaging with sparsity $K = 7$.

The enhanced AWI method, for all three choices of the sparsity parameter, exhibits a narrower localization of the wavefront and the echoes. The propagation of the wavefront can thus readily be tracked by eye or image processing tools, because a sharp contrast of the wavefront to its surrounding is achieved. Imaging results of the enhanced scheme exhibit considerably less noise and speckles throughout the region of interest. This successful suppression of noise is an eminent improvement in imaging quality compared to the conventional schemes. Results for the enhanced AWI method appear qualitatively similar, regardless of the sparsity parameter, although for larger $K$ additional speckles occur. Since the representation of the wavefield is compact, any perturbation of the wavefront due to reflections or interference can be detected easily. Due to the sensitivity of the enhanced scheme some pre-echoes emerge, for example in the first column (from the left) in Fig. 3. Since the smoothing during our signal processing involves future data points with respect to time these early echoes are generated. A disadvantage of all approaches employing an amplitude envelope is the loss of the ability to resolve the internal structure of the wavefront. For example in the fifth, most right column in Fig. 3 the position of the top right scatterer is best visualized by the classical AWI technique. Nevertheless, the orientation of this very same scatterer can also be deduced from the reflections, which are appreciable in the third, fourth and fifth columns (from the left) generated by

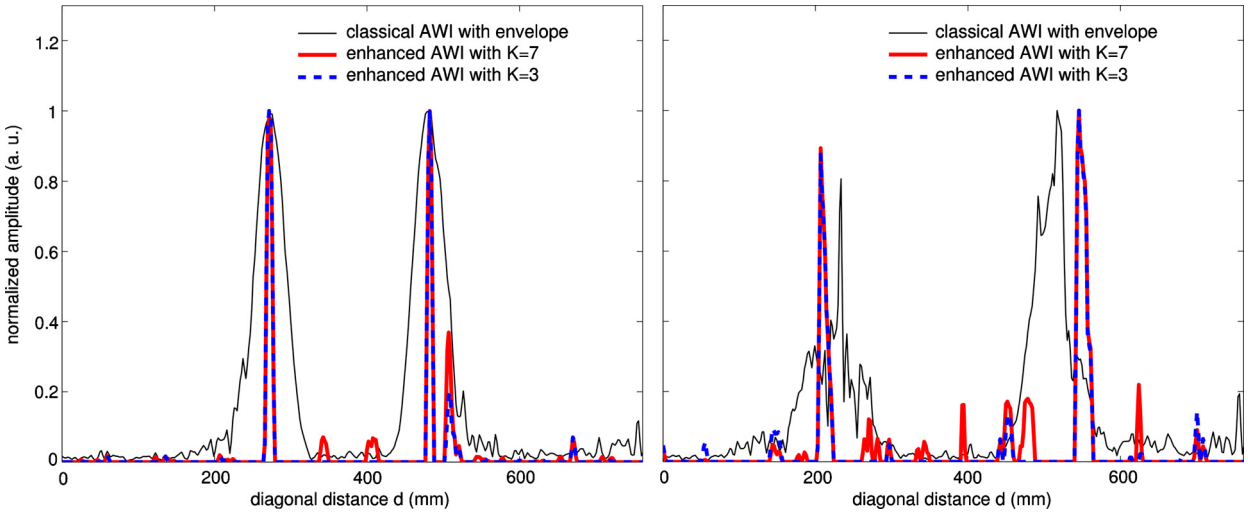


**Fig. 4.** Cross-section through wavefield snapshots at 84 µs (left) and 118 µs (right). Comparison of cross-sections for the classical method with amplitude envelope and the enhanced method with sparsity $K = 3$ and $K = 7$. The location of the cross-section is depicted by white lines in Fig. 3. The amplitude of the three distinct cross-sections is normalized.

the enhanced imaging scheme, especially in the lower row where $K = 7$. All methods considered here, fail however to make the bottom left scatterer visible, due to its orientation parallel to the propagation direction of the wavefront.

In order to highlight the improvement of our enhanced method, Fig. 4 illustrates the wavefield cross-sections of the classical method (employing amplitude envelopes) and the enhanced wavefield imaging with different sparsity levels. These diagonal cross-sections are taken from the first and the last column of Fig. 3. In general, the sparse time-domain representation within the enhanced framework leads to a spatial wavefield with less spread and thus to an improved localization. At the same time the improved scheme suppresses noise. However, for larger $K$ some clutter emerges. On the left-hand side of Fig. 4 the third highest peak for the enhanced methods corresponds to one of the aforementioned pre-echoes, which are visible due to temporal smoothing and the high spatial resolution. On the right-hand side of Fig. 4 the compact reflection due to the bottom right scatterer, which is appreciable in the fifth column of Fig. 3, is not present in the cross-section, because it does not lie exactly on the diagonal.

## 4. Conclusions

In this paper, we proposed a wavefield deconvolution technique that improves the assessment of structural defects in Lamb wave based structural health monitoring. The technique is formulated as a compressed sensing problem and generates spike trains of the measured narrowband ultrasound A-scans. It was shown that spurious peaks with small amplitudes, which are a side-effect of the orthogonal matching pursuit method, can be smoothed out by a moving average filter. Hence, the user-defined parameter is of minor importance here. The robustness of the deconvolution preprocessor was demonstrated by 32,942 SLDV measurements on an aluminum plate having four cracks of different orientation. In comparison to the wavefield animation with the conventional radio-frequency and envelope-detected waveforms, a clearer view of the defect was demonstrated.

A characteristic property of the method is the model-based nature so that it can be applied non-only to aluminum but also to composite structures using a suitable dictionary. Moreover, the method does not require a well understanding of the structure to be monitored, which is generally required for frequency-wavenumber methods. In the future, we will perform parametric studies to evaluate various defects in metallic and composite structures. Furthermore, we will explore the ability to reduce drastically the amount of measurement data needed within the enhanced approach.

## Acknowledgements

We acknowledge Prof. Fritzen (University of Siegen, Germany) for providing the SLDV.

## References

[1] Moll J, Fritzen C-P. Guided waves for autonomous online identification of structural defects under ambient temperature variations. J Sound Vib 2012;331(20):4587–97.
[2] Keulen CJ, Yildiz M, Suleman A. Damage detection of composite plates by lamb wave ultrasonic tomography with a sparse hexagonal network using damage progression trends. Shock Vib 2014;2014:1–8. http://dx.doi.org/10.1155/2014/949671. http://www.hindawi.com/journals/sv/2014/949671/.
[3] Yu L, Giurgiutiu V. In-situ optimized PWAS phased arrays for lamb wave structural health monitoring. J Mech Mater Struct 2007;2(3):459–87. http://dx.doi.org/10.2140/jomms.2007.2.459. http://msp.org/jomms/2007/2-3/p04.xhtml.

[4] Moll J, Schulte R, Hartmann B, Fritzen C-P, Nelles O. Multi-site damage localization in anisotropic plate-like structures using an active guided wave structural health monitoring system. Smart Mater Struct 2010;19(4):045022 (16 p.).
[5] Hall JS, Michaels JE. Minimum variance ultrasonic imaging applied to an in situ sparse guided wave array. IEEE Trans Ultrason Ferroelectr Freq Control 2010;57(10):2311–23. http://dx.doi.org/10.1109/TUFFC.2010.1692. http://ieeexplore.ieee.org/lpdocs/epic03/wrapper.htm?arnumber=5587413.
[6] Staszewski W, Lee B, Mallet L, Scarpa F. Structural health monitoring using scanning laser vibrometry: I. Lamb wave sensing. Smart Mater Struct 2004;13:251–60.
[7] Michaels TE, Michaels JE. Application of acoustic wavefield imaging to non-contact ultrasonic inspection of bonded components. In: AIP Conf Proc, vol. 820. IOP Institute of Physics Publishing Ltd.; 2006. p. 1484.
[8] Flynn EB, Chong SY, Jarmer GJ, Lee J-R. Structural imaging through local wavenumber estimation of guided waves. Nondestruct Test Eval Int 2013;59:1–10. http://dx.doi.org/10.1016/j.ndteint.2013.04.003. http://linkinghub.elsevier.com/retrieve/pii/S0963869513000595.
[9] Moll J, Rezk-Salama C, Schulte R, Klinkert T, Fritzen C-P, Kolb A. Interactive simulation and visualization of lamb wave propagation in isotropic and anisotropic structures. 9th international conference on damage assessment of structures J Phys Conf Ser 2011;305:012095.
[10] Sohn H, Dutta D, Yang JY, DeSimio M, Olson S, Swenson E. Automated detection of delamination and disbond from wavefield images obtained using a scanning laser vibrometer. Smart Mater Struct 2011;20(4):045017. http://dx.doi.org/10.1088/0964-1726/20/4/045017. http://stacks.iop.org/0964-1726/20/i=4/a=045017?key=crossref.3e778b0433c93f729ea38bb89a0fea3b.
[11] Ostachowicz W, Wandowski T, Malinowski P. Damage detection using laser vibrometry. In: 2nd international symposium on NDT in aerospace 2010. 2010. p. 1–8.
[12] Lee J-R, Ciang Chia C, Park C-Y, Jeong H. Laser ultrasonic anomalous wave propagation imaging method with adjacent wave subtraction: algorithm. Opt Laser Technol 2012;44(5):1507–15. http://dx.doi.org/10.1016/j.optlastec.2011.12.008. http://linkinghub.elsevier.com/retrieve/pii/S0030399211003963.
[13] Tian Z, Yu L. Lamb wave frequency-wavenumber analysis and decomposition. J Intell Mater Syst Struct, http://dx.doi.org/10.1177/1045389X14521875. http://jim.sagepub.com/cgi/doi/10.1177/1045389X14521875.
[14] Ruzzene M. Frequency-wavenumber domain filtering for improved damage visualization. Smart Mater Struct 2007;16(6):2116–29. http://dx.doi.org/10.1088/0964-1726/16/6/014. http://stacks.iop.org/0964-1726/16/i=6/a=014?key=crossRef.927b52dfadd700e4be090ee810a0607a.
[15] Rogge MD, Leckey CA. Characterization of impact damage in composite laminates using guided wavefield imaging and local wavenumber domain analysis. Ultrasonics 2013;53(7):1217–26. http://dx.doi.org/10.1016/j.ultras.2012.12.015. http://linkinghub.elsevier.com/retrieve/pii/S0041624X13000607.
[16] De Marchi L, Moll J, Marzani A. A sparsity promoting algorithm for time of flight estimation in guided waves-based SHM. In: 7th European workshop on structural health monitoring (EWSHM). 2014. p. 583–90. https://hal.inria.fr/hal-01020402.
[17] Moll J, Heftrich C, Fritzen C-P. Time-varying inverse filtering of narrowband ultrasonic signals. Struct Health Monit 2011;10(4):403–15.
[18] Perelli A, Ianni T, Marzani A, Marchi L, Masetti G. Model-based compressive sensing for damage localization in lamb wave inspection. IEEE Trans Ultrason Ferroelectr Freq Control 2013;60(10):2089–97. http://dx.doi.org/10.1109/TUFFC.2013.2799. http://ieeexplore.ieee.org/lpdocs/epic03/wrapper.htm?arnumber=6604540.
[19] Wei L, Huang Z-y, Que P-w. Sparse deconvolution method for improving the time-resolution of ultrasonic NDE signals. Nondestruct Test Eval Int 2009;42(5):430–4. http://dx.doi.org/10.1016/j.ndteint.2009.01.009. http://linkinghub.elsevier.com/retrieve/pii/S0963869509000267.
[20] Li X, Li X, Wang R. Compressed sensing based ultrasonic nondestructive testing by the use of sparse deconvolution. Chin J Electron 2013;22(2):405–9.
[21] Yu C, Zhang C, Xie L. An envelope signal based deconvolution algorithm for ultrasound imaging. Signal Process 2012;92(3):793–800. http://dx.doi.org/10.1016/j.sigpro.2011.09.024. http://linkinghub.elsevier.com/retrieve/pii/S0165168411003410.
[22] Zhang G-M, Zhang C-Z, Harvey DM. Sparse signal representation and its applications in ultrasonic NDE. Ultrasonics 2012;52(3):351–63. http://dx.doi.org/10.1016/j.ultras.2011.10.001. http://linkinghub.elsevier.com/retrieve/pii/S0041624X11002162.
[23] Candès EJ, Wakin MB. An introduction to compressive sampling. IEEE Signal Process Mag 2008;25(2):21–30.
[24] Strohmer T. Measure what should be measured: progress and challenges in compressive sensing. IEEE Signal Process Lett 2012;19(12):887–93.
[25] Donoho DL, Elad M, Temlyakov VN. Stable recovery of sparse overcomplete representations in the presence of noise. IEEE Trans Inf Theory 2006;52(1):6–18.
[26] Pati YC, Rezaiifar R, Krishnaprasad PS. Orthogonal matching pursuit: recursive function approximation with applications to wavelet decomposition. In: Signals, systems and computers, 1993. 1993 conference record of the twenty-seventh asilomar conference on IEEE. 1993. p. 40–4.
[27] Tropp J, Gilbert A. Signal recovery from random measurements via orthogonal matching pursuit. IEEE Trans Inf Theory 2007;53(12):4655–66. http://dx.doi.org/10.1109/TIT.2007.909108.
[28] Rossi M, Haimovich AM, Eldar YC. Compressive sensing with unknown parameters. In: Signals, systems and computers (ASILOMAR). 2012 conference record of the forty sixth ASILOMAR conference on IEEE. 2012. p. 436–40.